Research article

Peng Yin, Wenli Bao, Lingfeng Gao*, Jianlong Kang, Rui Huang, Xin Wang, Songrui Wei*, Yanqi Ge* and Han Zhang

Performance analysis of photo-electrochemical photodetector based on liquid-phase exfoliation few-layered graphdiyne nanosheets

https://doi.org/10.1515/nanoph-2021-0074
Received February 22, 2021; accepted July 13, 2021;
published online August 11, 2021

Abstract: The band gap of two-dimensional (2D) materials become a hot issue for photoelectric detection. Recently, public attention is thoroughly aroused as to the remarkable electrical transport characteristic and super photoresponse of 2D graphdiyne. The simulation results show that the photoresponse can be adjusted in various solutions based on the graphdiyne nanosheets with different sizes and thicknesses. Based on few-layered graphdiyne nanosheets prepared by a liquid-phase exfoliation method, a photo-electrochemical (PEC)-type few-layered graphdiyne photodetector is demonstrated in this paper. A group of PEC tests are carried out in neutral solution to verify the simulation results. The as-prepared graphdiyne photodetector possesses high photocurrent density, effective responsivity and excellent cycle stability in condition of KCl electrolyte and solar illuminance. The detectivity of the PEC-type graphdiyne photodetector can be easy to adjust by altering electrolyte concentration and other corresponding parameters, which indicates the proposed equipment can be a good candidate for photoelectric detection.

Keywords: graphdiyne; long-term stability; neutral environment; photodetection; photoelectrochemical.

***Corresponding authors: Lingfeng Gao**, Institute of Microscale Optoelectronics, Collaborative Innovation Centre for Optoelectronic Science & Technology, International Collaborative Laboratory of 2D Materials for Optoelectronics Science and Technology of Ministry of Education, Key Laboratory of Optoelectronic Devices and Systems of Ministry of Education and Guangdong Province, College of Physics and Optoelectronic Engineering, Shenzhen Key Laboratory of Micro-Nano Photonic Information Technology, College of Physics and Optoelectronics Engineering, Guangdong Laboratory of Artificial Intelligence and Digital Economy (SZ), Shenzhen University, Shenzhen 518060, P.R. China; and College of Material, Chemistry and Chemical Engineering, Hangzhou Normal University, No. 2318 Yuhangtang Rd., Cangqian, Yuhang District, Hangzhou, 311121, P.R. China; and **Songrui Wei** and **Yanqi Ge**, Institute of Microscale Optoelectronics, Collaborative Innovation Centre for Optoelectronic Science & Technology, International Collaborative Laboratory of 2D Materials for Optoelectronics Science and Technology of Ministry of Education, Key Laboratory of Optoelectronic Devices and Systems of Ministry of Education and Guangdong Province, College of Physics and Optoelectronic Engineering, Shenzhen Key Laboratory of Micro-Nano Photonic Information Technology, College of Physics and Optoelectronics Engineering, Guangdong Laboratory of Artificial Intelligence and Digital Economy (SZ), Shenzhen University, Shenzhen 518060, P.R. China, E-mail: gaolingfeng@szu.edu.cn (L. Gao), weisongrui@126.com (S. Wei), geyanqi@hotmail.com (Y. Ge)
Peng Yin, Institute of Microscale Optoelectronics, Collaborative Innovation Centre for Optoelectronic Science & Technology, International Collaborative Laboratory of 2D Materials for Optoelectronics Science and Technology of Ministry of Education, Key Laboratory of Optoelectronic Devices and Systems of Ministry of Education and Guangdong Province, College of Physics and Optoelectronic Engineering, Shenzhen Key Laboratory of Micro-Nano Photonic Information Technology, College of Physics and Optoelectronics Engineering, Guangdong Laboratory of Artificial Intelligence and Digital Economy (SZ), Shenzhen University, Shenzhen 518060, P.R. China; and School of Materials Science and Engineering, Hanshan Normal University, Chaozhou, Guangdong 521041, P.R. China. https://orcid.org/0000-0001-6355-3516
Wenli Bao, Jianlong Kang and Han Zhang, Institute of Microscale Optoelectronics, Collaborative Innovation Centre for Optoelectronic Science & Technology, International Collaborative Laboratory of 2D Materials for Optoelectronics Science and Technology of Ministry of Education, Key Laboratory of Optoelectronic Devices and Systems of Ministry of Education and Guangdong Province, College of Physics and Optoelectronic Engineering, Shenzhen Key Laboratory of Micro-Nano Photonic Information Technology, College of Physics and Optoelectronics Engineering, Guangdong Laboratory of Artificial Intelligence and Digital Economy (SZ), Shenzhen University, Shenzhen 518060, P.R. China. https://orcid.org/0000-0002-9131-9767 (H. Zhang)
Rui Huang, School of Materials Science and Engineering, Hanshan Normal University, Chaozhou, Guangdong 521041, P.R. China
Xin Wang, School of Engineering, Monash University Malaysia, Jalan Lagoon Selatan, 47500 Bandar Sunway, Selangor, Malaysia

1 Introduction

Light detection is an indispensable behavior where the optical signal can be converted into an electrical signal and it plays an important part in transducer, communication and spectroscopy. In recent years, two-dimensional (2D) materials featured by mono- or few-layers become a popular part in lasers, photodetectors, biomedicine and other fields. In the field of optoelectronics, there is growing concern about 2D materials because of their unique electrical and optical characteristics, which come from the ultrathin flat construction. Because of zero bandgap structure and high carrier mobility, graphene has been taken as an object of study. The charge carriers in graphene are similar to massless Dirac fermions [1]. Graphene also has more advantages on weight and robustness than traditional indium tin oxide (ITO), and has better flexibility [2]. In addition, graphene can be a transparent conductor owing to its lower absorption (<2.3%) in the visible region [2–4] and it has talent in broadband photodetection because of its wide absorption. However, the graphene-based photodetectors have lower responsivity caused by low absorption and nonexistent photoconductive gain [1], which restricts their further applications [2]. The absence of band gap gives rise to no electronic states and high dark current, which is disadvantage for photodetectors [3]. Although several approaches can change the band structures of graphene [4], the applications of photodetection still need further discussion. After graphene, black phosphorus (BP) has been widely studied and it reveals excellent talent in photoelectronic devices [5–9], sensors [10, 11], lithium ion batteries [5, 12, 13], solar cells [14, 15], and biomedicine [16–18] owing to its tunable direct band gap [19, 20], high electronics ON/OFF ratio [21] and high carrier mobility [22]. Nonetheless, the unstable problem has plagued the BP under ambient conditions, which gives rise to the failure of electronic and optical properties [23–25]. To overcome the aforementioned problems, several countermeasures have been introduced, such as adding capping layers [26, 27], ligand surface coordination [28, 29], fluorination [30] and covalent aryl diazonium functionalization [31]. But for all this, how to obtain BP-based photoelectrochemical photodetectors with the favourable performance is still difficult. In order to overcome the unstability of BP, blackphosphorus-analogues (BPAs) have been especially noticeable because of tunable band gap, high carrier mobility and high ON/OFF ratio with a structure similar to BP but more stable under ambient conditions. Huang et al. studied different kinds of BPAs [32–36] and realized favourable photodetection function and stability. Pletikosic et al. [37] reported SnSe material and achieved high carrier mobility and excellent stability under ambient conditions. Nevertheless, these advantages of BPAs above only can be obtained under specific conditions. Especially in neutral or acidic aqueous solutions, the strength of the photoelectric detected signal is very weak [38, 39]. Apart from graphene and BP, transition metal dichalcogenides (TMDs) possess high carrier mobilities and low dark currents [40]. By reason of the various band gaps versus thicknesses, the electric and optical attributes can be tailored by changing the cutoff wavelength [41, 42]. Recently, transition-metal carbides and/or nitrides (known as MXenes) have emerged and widely investigated [43–46]. In addition, non-layered 2D materials have been favored by researchers [24, 47–49] owing to their unique properties of affluent dangling bonds, particular structural distortion, adjustable band gap, and high carrier mobility [50–54]. The fabrication of non-layered 2D materials usually adopts the van der Waals epitaxial method and chemical vapor deposition [55]. However, for the fabricated methods above, harsh preparation process is a fairly challenge including extreme temperature and vacuum environment.

As a new carbon family material, graphyne possesses distinguished optical and electronic characteristics based on its special *sp*- and sp^2-hybridized carbon structure [56]. However, it for a long time was stagnant since the first graphyne has presented in 1987. In 2010, large-area graphdiyne films were fabricated for the first time by the Glaser–Hay cross-coupling reaction [57]. Unlike graphene with zero band gap, first principle calculations confirmed that graphyne has an inborn band gap energy, where the minimal band gap is about from 0.46 to 1.22 eV with various approaches and exchange correlation functions [57, 58]. Graphynes can be divided into α-graphyne, β-graphyne, γ-graphyne and so on, in which the γ-graphyne also means graphdiyne. Graphdiyne has been revealed abundant applications including separation and purification, energy storage and transfer, catalysts, electronic and magnetism, biomedicine and therapy, even in detector fields while the issue in electrochemical interfaces can be solved via employing GDY [59–62]. Li et al. reported about hydrogen evolution via anchoring zero valence single atoms of nickel and iron on GDY, generating of ammonia and hydrogen on a GDY-based catalyst, obtaining high-performance organic batteries by *in situ* weaving GDY nanocoatings and GDY-cobalt nitride (GDY/Co_2N) as a catalyst for the electrochemical nitrogen reduction reaction (ECNRR) [63–67]. Zhang et al. [68] revealed that GDY graphdiyne exhibits outstanding nonlinear properties in nonlinear photonic devices, such as Kerr switcher, modulator, and wavelength converter. In view of the modified structure of

sp^2-hybridized carbon, graphdiyne possesses higher stability and more outstanding carrier mobility than graphene. However, to the best of our knowledge, high-performance photo-electrochemical (PEC) photodetector of graphdiyne and the band structure and adsorption energy of OH and H_2O for the different shapes of graphdiyne nanosheets have been rarely researched.

In this paper, a simulation was carried out to reveal various photoresponse performances based on graphdiyne nanosheets with different sizes and thicknesses. A facile liquid exfoliation approach was employed to prepare graphdiyne nanosheets which were used to fabricate PEC-type photodetector with outstanding photoresponse. The cycling performance and long-term stability tests show that graphdiyne photodetector possesses attractive durability in condition of chloride environment. In addition, the photoelectronic performance of graphdiyne PEC-type photodetector in different KCl concentrations was investigated.

2 Simulation

Firstly, a first principle calculation based on density functional theory (DFT) is performed to investigate the photocurrent of graphdiyne in photoelectrochemical experiment. Apart from the band structure which is related to the excitation of photoelectrons, we also calculate the free energy of oxygen evolution reaction (OER) on graphdiyne to exclude the effect of electrolysis of water. Figure 1a and b are the band structures of monolayer and bilayer graphdiyne. It can be seen that the band gap decreases with the increase of layer number, which is a general phenomenon in 2D materials. For a semiconductor with smaller band gap, the electrons are easier to be excited by photons and the photocurrent will be enhanced. The samples in experiment are about 10 layers and the band gap should be smaller. Based on our calculation about the OER reaction, the adsorption energy of OH^- on graphdiyne is about −0.56 eV. So, OH^- should be easy to adsorb on the surface of graphdiyne in alkaline environment. According to the reactive molecular dynamics simulations revealed by Jhon et al. [69], the mechanical properties of MXene can be enhanced by surface terminations due to the improved stiffness. It is supposed that the graphdiyne with terminations possess excellent mechanical stability, which will be experimentally confirmed in the following experiments. We calculated the band structure of four-layer graphdiyne with and without the adsorption of OH^- and the corresponding results are shown in Figure 1c and d respectively. It can be seen that the four-layer graphdiyne without OH is a semiconductor while it transforms to a metal when OH is adsorbed on it. This indicates that the layered graphdiyne may have a better performance in neutral or acid environment than that in alkaline one.

Apart from the current when light is on, the dark current is also an important parameter for photodetector because it determines the smallest detectable signal as described by the following equation.

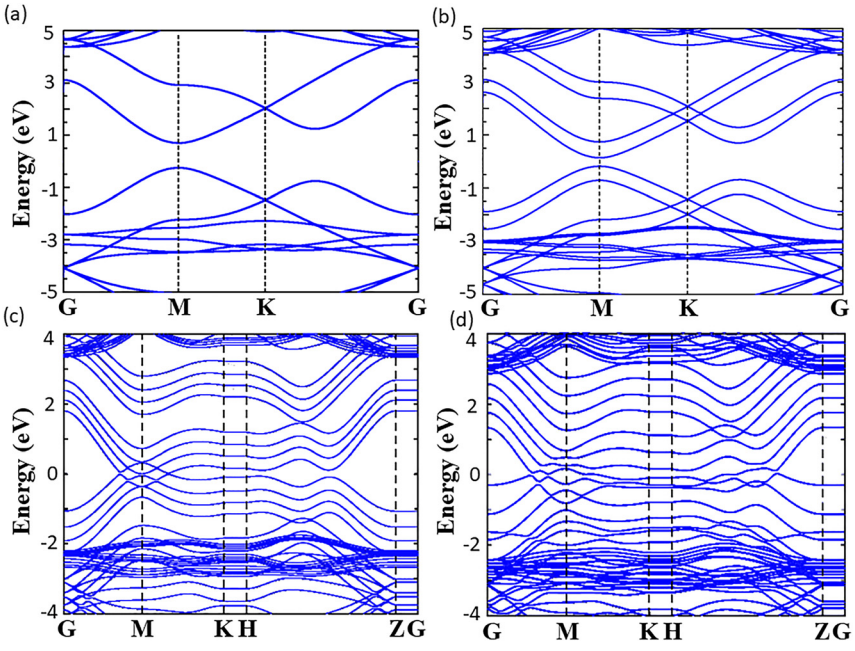

Figure 1: The band structure of (a) monolayer and (b) bilayer graphdiyne; the band structure of (c) four-layer graphdiyne with the adsorption of OH^- and (d) without the adsorption of OH^-.

$$D^* = R_{ph} \times \left(\frac{s}{2q \times I_{off}} \right)^{0.5} \quad (1)$$

The standard electrode potential is about 0.4 and 0.8 V respectively in pH = 14 and pH = 7 solutions. So, when the voltage on anode is large enough and the overpotential of anode material is small enough, there may be OER reaction on the anode. Therefore, we calculate the free energy of OER reaction on layered graphdiyne and the corresponding results are shown in Figure 2.

$$* + H_2O = *OH + H^+ + e^- \quad (2)$$

$$*OH = *O + H^+ + e^- \quad (3)$$

$$*O + H_2O = *OOH + H^+ + e^- \quad (4)$$

$$*OOH = * + O_2 + H^+ + e^- \quad (5)$$

Under the neutral condition, pH = 7 and the standard electrode potential is adjusted to be 0.8165 V. All the calculated free energies in this work have been corrected with vibrational energy and entropy. It is obvious that the first step needs the largest overpotential (1.93 V) and it is the rate determining step. But in fact, the applied voltage on graphdiyne anode is only 0.6 V in experiment. Therefore, there should be no OER reaction on graphdiyne. This result is consistent with the experimental observations. On the cathode, there are many bubbles when the voltage is applied, and the process is lasting. So, there should be hydrogen evolution reaction (HER). On the anode, however, only a few bubbles are observed, and we ascribe these bubbles to the air or vapor in the solution.

In conclusion, the calculated band structure implies that the photo response of layered graphdiyne should be strong and it may have a better performance as a photodetector in acid or neutral environment than in alkaline environment. On the other hand, the possibility of OER reaction on the anode is excluded and the dark current will not be contributed by the OER reaction. It means that layered graphdiyne will have a large D^* and high sensitivity. Therefore, we suppose that layered graphdiyne should be a good candidate for photodetector especially in acid or neutral environment.

3 Results and discussion

Based on the simulation results, the synthetic approach of the graphdiyne nanosheets is modified (detailed in Section 5) and the sample is achieved with thin and large morphology which is hoped to show better photoresponse ability in neutral or acidic environment. Figure 3(a) represents the outline and structure of the as-prepared graphdiyne by scanning electron microscopy (SEM), which is recorded on a JEOL JSM-7000F electron microscope (Japan). The microstructure of nanosheets can be observed obviously. Figure 3(b) shows a plicated layer outline of graphdiyne by the transmission electron microscopy (TEM) with the type of FEI Tecnai F20 instrument (USA). This indicates that the as-prepared graphdiyne after ultrasound operation can be a 2D material with more distinct morphology than those in other references [70, 71]. The diversity of chemical bonding in the same carbon layer or among different carbon layers leads to the plicated morphology. The as-prepared graphdiyne nanosheets possess several obvious chemical and physical characteristics including wide surface area, high carrier mobility and good toughness, etc. Figure 3(c) represents the high-resolution transmission electron microscopy (HRTEM) image of graphdiyne with the obvious lattice fringes, which indicates well crystallinity of the obtained graphdiyne nanosheets. Figure 3(c) inset shows the clearly diffraction spots from the selected area electron diffraction

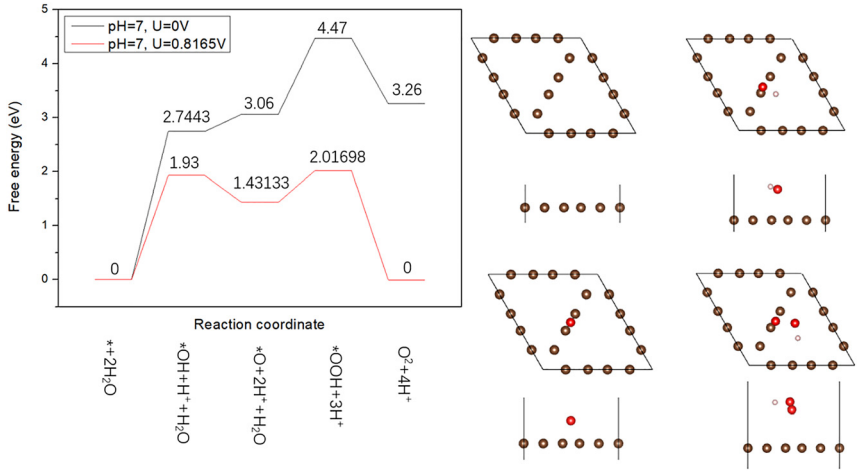

Figure 2: Free energy of four steps of oxygen evolution reaction (OER) reaction on the graphdiyne as the anode.

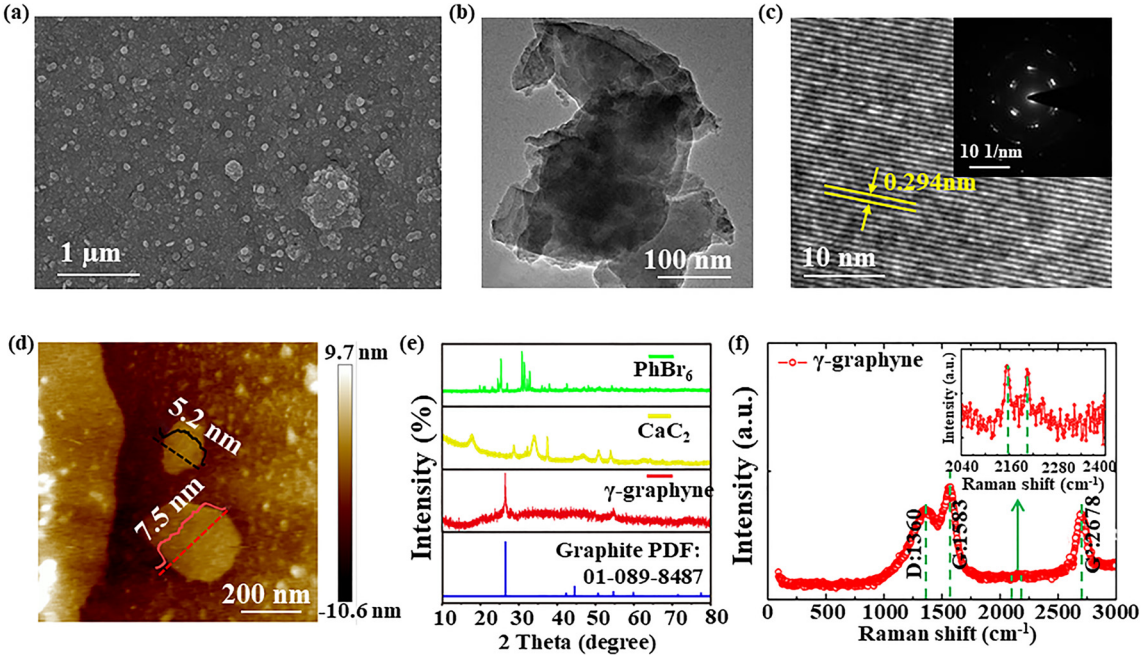

Figure 3: (a) scanning electron microscopy (SEM) image, (b) transmission electron microscopy (TEM) image, (c) high-resolution transmission electron microscopy (HRTEM) image of exfoliated graphdiyne (inset is SEAD pattern), (d) atomic force microscope (AFM) image relative cross-sectional analysis of as-prepared graphdiyne nanosheets, (e) X-ray diffraction (XRD) pattern of as-prepared graphdiyne nanosheets and (f) Raman spectra of exfoliated graphdiyne nanosheets on SiO_2/Si substrate.

(SAED) image, which indicates the nanocrystal morphology and well-structured crystallinity of the obtained graphdiyne nanosheets. The SAED patterns of various stacking modes of graphdiyne have been calculated [72]. The corresponding lattice distance is the same as the lattice stacking mode. The diffraction spots are tested and various lattice distances are observed. Figure 3(d) shows the atomic force microscope (AFM) image of the as-prepared graphdiyne nanosheets on the Si/SiO_2 substrates. The slice profile of the graphdiyne nanosheets can be observed and measured. The corresponding profile of the graphdiyne nanosheets shows that the thickness of the nanosheets is less than 10 nm. Figure 3(e) shows the X-ray diffraction (XRD) patterns of $PhBr_6$, CaC_2, graphdiyne and graphite PDF card (JCPDS NO.01-089-8487). This XRD patterns are tested on Panalytical X′ Pert X-ray diffractometer (Holland) fitted with Cu-Kα radiation in condition of 40 kV accelerating voltage and 40 mA applied current. The rest of the unreacted $PhBr_6$ and CaC_2 are entirely eliminated with the purification operation because of the absence of their characteristic diffraction peaks. The obtained graphdiyne represents two obvious diffraction peaks at the 2θ of 26 and 54°, which are consistent with the crystal planes of (002) and (004) [70]. In addition, several little diffraction peaks are shown in XRD patterns of graphdiyne owing to the graphite. The XRD patterns of graphdiyne demonstrate fixed carbon content in the obtained graphdiyne in standard graphitized form. In order to identify the chemicals surrounding the carbon materials, Raman spectra is employed on a Raman spectrometer (Renishaw, UK) with a 325 nm He–Cd excited laser source, as shown in Figure 3(f). Two predominant peaks in Raman spectra of graphdiyne are depicted at 1360 cm^{-1} (D band) and 1583 cm^{-1} (G band), respectively. The presence of D band is because of several flaws and chaotic constructions in carbonaceous materials. However, the occurrence of G band indicates the first-order Raman expanding for same-phase expanding shock of sp^2-cross-fertilized carbon in aromatic rings. In addition, there are two weak bands located at 2148 and 2204 cm^{-1} because of the vibration of conjugated ethynyl links originating from the vibration of *sp*-hybridized carbon [73].

In order to evaluate the photoresponse performance of graphdiyne, a group of photoelectrochemical test results has been depicted in Figure 4. The *C*–*V* curve is depicted by linear sweep voltammograms (LSV) in condition of 0.5 M KCl with a scanning speed of 10 mV s^{-1}, as shown in Figure 4a. The dark current density of the graphdiyne electrode is located above 0 A in condition of the bias potential of 0 V. The intensities of light and dark photocurrent increase versus the bias potential. In addition, intensity

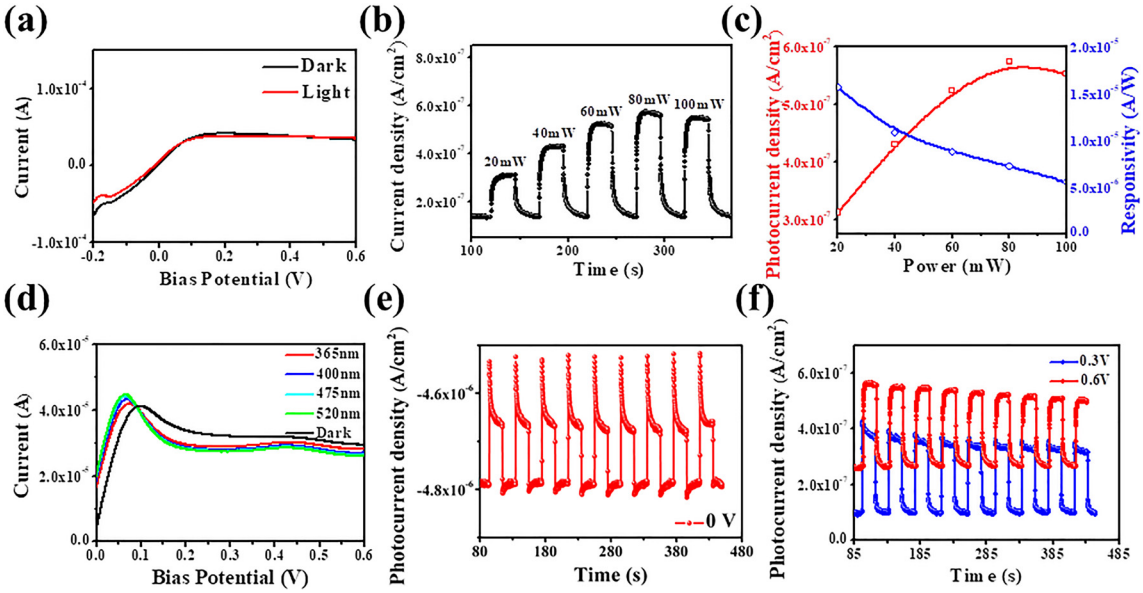

Figure 4: (a) Linear sweep voltammograms (LSV) tests of graphdiyne in 0.5 M KCl in the dark and light environments, respectively. (b) Photocurrent density of graphdiyne in condition of different illumination intensities in 0.5 M KCl. (c) Matching B-spline curve and calculated photoelectric responsivity versus irradiance power intensity in 0.5 M KCl. (d) LSV measurements of graphdiyne in 0.5 M KCl in condition of various wavelength. (e) Photocurrent density in condition of bias potential of 0 V in 0.5 M KCl, and (f) photocurrent density in condition of bias potential of 0.3 and 0.6 V under 0.5 M KCl.

and wavelength from incident light are two important parameters for the performance evaluation of photodetectors [74, 75]. The photocurrent density of graphdiyne nanosheets increases along with the power intensity of incident sunlight steadily in condition of the bias potential of 0 V, as shown in Figure 4b. The photocurrent density achieves 650 nA·cm^{-2} in condition of the power intensity of 100 mW·cm^{-2}, which is two times higher than that at 20 mW·cm^{-2}. In addition, the photocurrent density (I_p) of graphdiyne photodetector is proportional to P^{θ} where P represents the power intensity of incident sunlight and θ represents the relationship between the tapping and recombination processes of the photocarriers [76]. To study the photoresponse performance of graphdiyne nanosheets at a deeper level, the photoelectric responsivity versus irradiance power intensity is depicted in Figure 4c, where the responsivity can be expressed by [77]:

$$R = \frac{I}{J_{\text{light}}} \tag{6}$$

where I and J_{light} are the photocurrent density and the irradiance intensity, respectively. The photoelectric responsivity of graphdiyne nanosheets increases along with the irradiance power intensity from 20 to 100 mW·cm^{-2}. The photocurrent density versus bias potential in condition of different irradiation wavelengths is depicted in Figure 4d. The current density increases first, but it gradually decreases after it reaches max value along with the bias potential, while the photocurrent density remains steady growth in the vicinity of the zero bias potential, which is consistent with the absorption spectra of graphdiyne. The above results show that graphdiyne possesses steady responsivity and stable sensitivity versus power density and wavelength of incident irradiation, which indicates the talent of graphdiyne in practical photodetectors.

In addition, an on/off switched phenomenon can be observed in Figure 4e by measuring with a self-powered PEC-type graphdiyne photodetector in condition of the bias potential of 0 V. With the on/off change of the incident irradiance periodically, the current density switches efficiently and steadily. A high on/off ratio can be achieved with the current density of −4650 nA·cm^{-2} for incident irradiation and −4800 nA·cm^{-2} for dark. When the applied bias potential is adjusted from 0 to 0.3 and 0.6 V, the photocurrent density of graphdiyne photodetector increases from −4650 to 350 and 550 nA·cm^{-2} as shown in Figure 4f, and the responsivity of graphdiyne photodetector increases from 15 to 19 and 37 μA·W^{-1}, respectively, which can be ascribed to the rasied PEC performance under positive potentials [78]. The above results indicate that the proposed graphdiyne photodetector possess high responsivity and effectively sensitivity without the help of external bias potential and the optimization of carrier concentration and photocurrent density versus the applied

bias potential [78]. A potential gradient within graphdiyne nanosheets can be established for accelerating separation between photogenerated holes and electrons under the applied bias potential. This illustrates the photodetection performance can be optimized by reasonable adjustment of bias potential. For comparison, several typical photodetectors are listed in Table 1 based on the nanosheets or flakes of BP [79–81], WSe_2 [82], MoS_2 [83–85], WS_2 [85]. Although the photoresponsivity of FET-based photodetector is more excellent than that of PEC-type photodetector, the prominent photoresoponse activity of PEC-type graphdiyne photodetector possesses huge possibilities and immense research worth.

Cycle stability and time stability are two key parameters to estimate the perdurability of graphdiyne photodetector in 0.5 M KCl. Figure 5a shows the current density versus potential after 50 and 100 cycles without obvious reduction and a minor offset owing to the decrease of functional material. After a long period of test, the time stability of the graphdiyne photodetector has been demonstrated with fairly stable photocurrent density which possesses slightest disturbance near 380 nA·cm^{-2}, as shown in Figure 5b. In fact, the photoresponse phenomenon of graphdiyne photodetector still remains stable and reasonable outside the on/off switching scope of 500 s, which indicates the high stability and reliability of graphdiyne in saline surroundings. The high stability of graphdiyne can be partly ascribed to the surficial terminations such as hydroxyl, as mentioned in the DFT calculation section. Similar results can be observed in our previous work, where the niobium carbide MXene with –OH/–F terminations also shows excellent stability [86]. Figure 5c depicts the photocurrent density of graphdiyne photodetector with different stored time of 1 h, one day, seven days and 30 days in condition of 0.5 M KCl. It is easy to see that the photocurrent density always maintains stable momentum without any obvious fluctuations after 1 h. Next, the photocurrent density creates decay during one day from 460 to 250 nA·cm^{-2}. The obvious decrement of the photocurrent density occurs after seven days and 30 days with the decline range of 210 and 235 nA·cm^{-2}, while the distinct on/off switching in both cases indicates the stability of the graphdiyne photodetector for long time.

In addition, the photoresponse performance of graphdiyne photodetector is tested with various concentrations of KCl electrolyte in condition of the incident irradiance of 100 mW cm^{-2} (Figure 6a). Figure 6b depicts the current density versus potential with different concentrations of KCl and NMP. The current density increases along with the applied bias potential especially beyond –0.4 V in above electrolytes except NMP. Furthermore, the maximal current intensity of graphdiyne photodetector occurs in 0.5 M KCl. The current increases from –0.8 to –0.35 mA versus the decline of the KCl concentration from 0.5 to 0.05 M in condition of the applied bias potential of –0.6 V. Besides, Figure 6c depicts the response time (t_{RES}) and recovery time (t_{REC}) of graphdiyne photodetector in different KCl concentrations, where the rise and decay from 10 to 90% and from 90 to 10% of its peak value, respectively. The time response coefficient of response (τ_{res}) and recovery (τ_{rec}) can be expressed by [87]

$$I(t) = I + A[\exp(-t/\tau)] \tag{7}$$

where a rapid response time of 0.5 s and a fast recovery time of 1.1 s are observed in 0.1 M KCl, respectively owing to the intrinsic property of fast electron transfer of graphdiyne. The relevant response results versus the concentration of KCl demonstrate the impacts of the concentration of electrolyte on the photocurrent density and the photoresponse performance in PEC type photodetectors. Finally, the electrochemical impedance spectrum (EIS) under different concentrations of KCl is investigated to demonstrate the photoresponse character ulteriorly (Figure 6d). Based on EIS, the contact resistances (R_s) can be calculated to indicate the resistance on interface between electrode and electrolyte, which suggests the electron transform

Table 1: Contrastive list of several test parameters for the as-prepared graphdiyne photodetector and others.

Materials	Conditions	Rise time	I_{on}/I_{off}	Responsivity	Ref.
γ-graphyne nanosheets	0.5 M KCl, 0.6 V	0.4 s	2	15–21 μA/W	This work
Few-layer BP flakes	Shottky-contact V_{ds} = –1 V, V_g = –20 V	5 ms	0.035	4.3×10^6 A/W	[79]
Few-layer BP flakes	Shottky-contact V_{ds} = –1 V, V_g = 10 V	–	3	3.5 mA/W	[80]
Few-layer BP	FET, V_{ds} = 0.2 V, V_g = 0 V	1 ms	10^{-3}	4.8 mA/W	[81]
WSe_2 nanosheets	Shottky-contact V_{ds} = 2 V, V_g = –60 V	10 s	–	180 A/W	[82]
MoS_2 nanosheets	Shottky-contact V_{ds} = 8 V, V_g = –70 V	4 s	–	880 A/W	[83]
Single-layer MoS_2	FET, V_{ds} = 1 V, V_g = 0 V	50 ms	~17	0.42 mA/W	[84]
MoS_2/WS_2 heterojunction	FET, V_{ds} = 2 V, V_g = 0 V	2 s	2.5	2.3 A/W	[85]

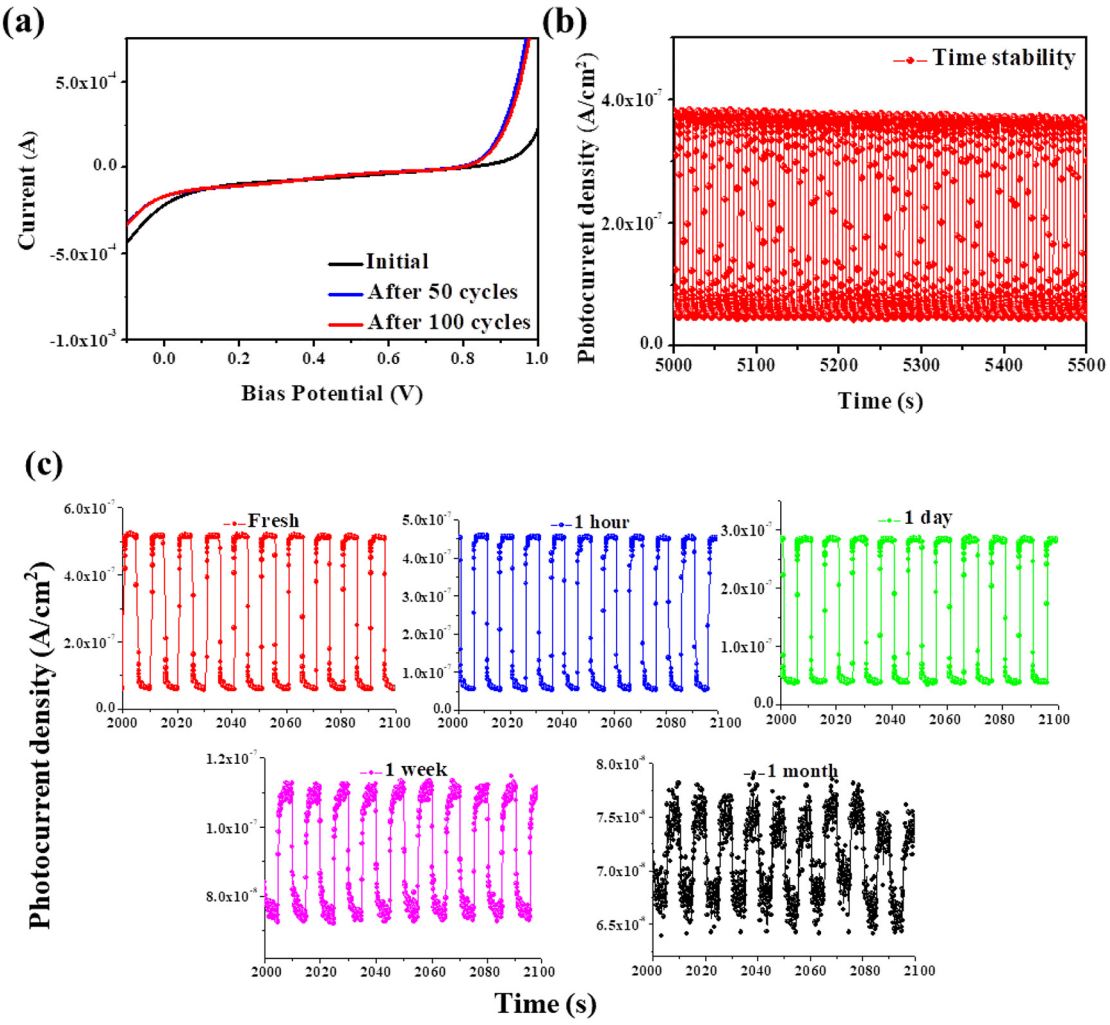

Figure 5: (a) Cycling stability experiments of graphdiyne photodetector in 0.5 M KCl. (b) Long-term photocurrent response tests of graphdiyne nanosheets-based photodetector. (c) Time stability measurements of graphdiyne photodetector after 1 h, 1 day, 1 week and 1 month under 0.5 M KCl.

efficiency. The values are calculated to be 16.2, 35.9, and 52.7 Ω in 0.5, 0.1, 0.05 M KCl, respectively. In Figure 6d, the graphdiyne nanosheets possess weak R_s under all salt environments. The R_s of the graphdiyne in 0.5 M KCl is smaller than that in concentrations of 0.1 and 0.05 M. It is worthy to note that R_s in 0.5 M KCl is much higher than that in low concentration environments mainly caused by a combination of conductivity and viscosity [88]. In addition, a continued slowdown in concentration of electrolyte will further weaken the photocurrent density and lose efficacy of PEC reaction. Therefore, under the equilibration together with photocurrent density and electron transform efficiency, the proposed graphdiyne nanosheets possess distinguished photoresponse performances with the saline solution in favor of graphdiyne photodetectors.

4 Conclusion

In summary, the photoresponse can be adjusted in various solutions based on the graphdiyne nanosheets with different sizes and thicknesses. 2D graphdiyne nanosheets have been presented with a businesslike liquid exfoliation approach and were succeed in employing for PEC-type photodetector. The as-prepared photodetector shows outstanding photocurrent density and photoresponse ability in condition of chloride environment under solar illuminance. The test results show that graphdiyne photodetector exhibits raised responsivity and cycling stability in condition of KCl solution. This paper shows the fundamental relationship between the photoresponse property and graphdiyne nanosheets based photodetectors, revealing its potential optoelectronic

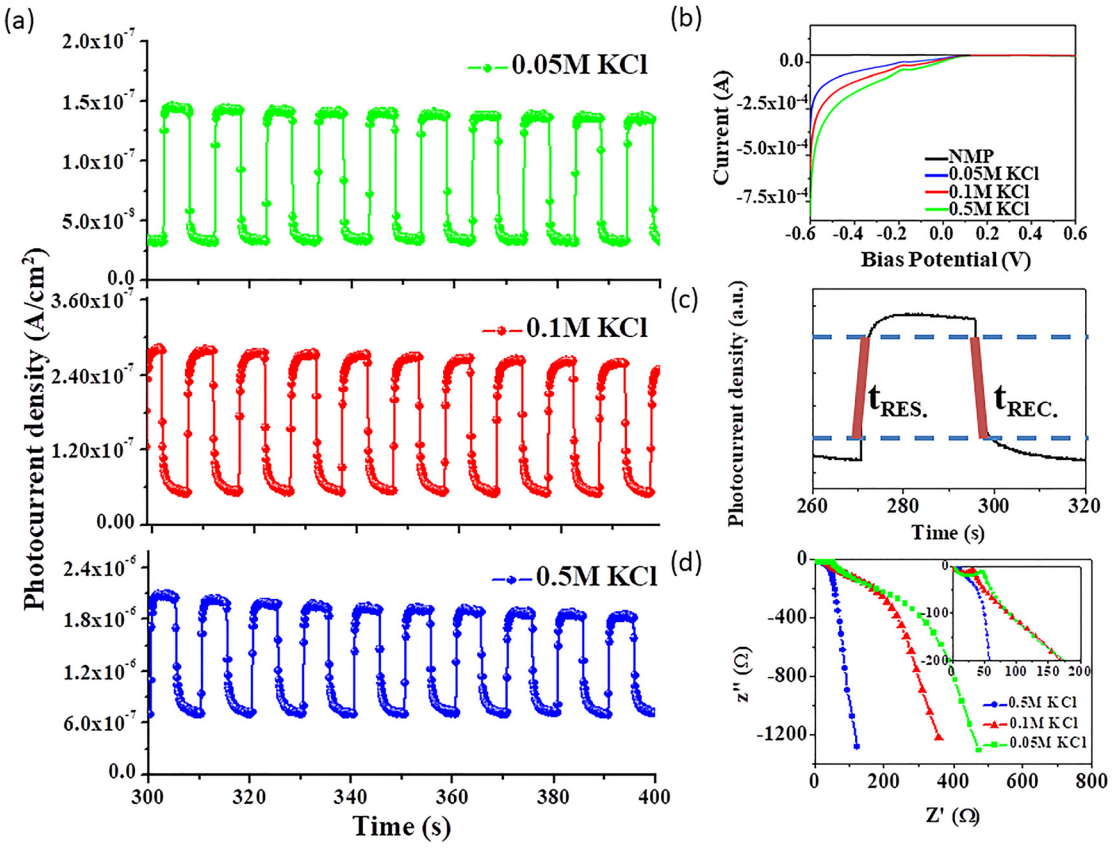

Figure 6: (a) Photocurrent measurements in various KCl concentration under dark and light environments. (b) Current versus bias potential under different KCl concentration and NMP solution. (c) Normalized photocurrent density under different time associates with exponential equation and the time constants for the response and recovery. (d) The impedance spectroscopic graphdiyne in various KCl concentration.

applications because of its intrinsical construction and photoelectronic ability.

5 Experimental section

The synthesis procedures of graphdiyne is followed Ref. [57], as shown in Figure 7a by Glaser coupling of the hexaethynylbenzene (HEB) monomer which was synthesized by Nigish coupling of hexabromobenzene and trimethylsilylacetylene zinc agent. To a solution of 1-heptyne (24 mmol) in THF (12 mL) at 0 °C was added 24 mmol of *n*-butyllithium in hexane. The solution was stirred for 5 min followed by the addition of anhydrous zinc chloride (24 mmol) dissolved in THF (24 mL) [89]. The mixture was stirred for an additional 15 min at room temperature. Then 1.1040 g (2.00 mmol) of hexabromobenzene, 600 mg (0.480 mmol) of $Pd(PPh_3)_4$, 30 mL of toluene were added into the zinc agent solution dropwise in a three-necked flask. The mixture was stirred under an argon atmosphere at 80 °C (oil bath temp.) for 3 days. After 24 mL of 1 M HCl was added, the reaction mixture was extracted with ethyl acetate. The combined organic layer was washed with brine and dried over anhydrous Na_2SO_4. The solvent was evaporated and the residue was then purified by column chromatography (silica gel, hexane: dichloromethane = 5:1) to yield 991 mg (63.2%) of hexakis [(trimethylsilyl)ethynyl] benzene as pale yellow solid. To a solution of 991 mg (1.50 mmol) in 340 mL THF was added 9.10 mL TBAF (1 M in THF, 9.1 mmol) and stirred at 8 °C for 10 min. The solution was then diluted with ethyl acetate and washed with brine and dried with anhydrous Na_2SO_4. The solvent was removed in vacuo and the deprotected material (202 mg, 62 %) was rediluted with 560 mL pyridine dividing into three flask and added slowly over 24 h to a solution of copper foils in 380 mL pyridine via constant pressure drop funnel at 60 °C and stirred under a nitrogen atmosphere at 60 °C for two days. Upon completion copper foils were washed with acetone and DMF and a black film was obtained on the copper foil, as shown in Figure 7b.

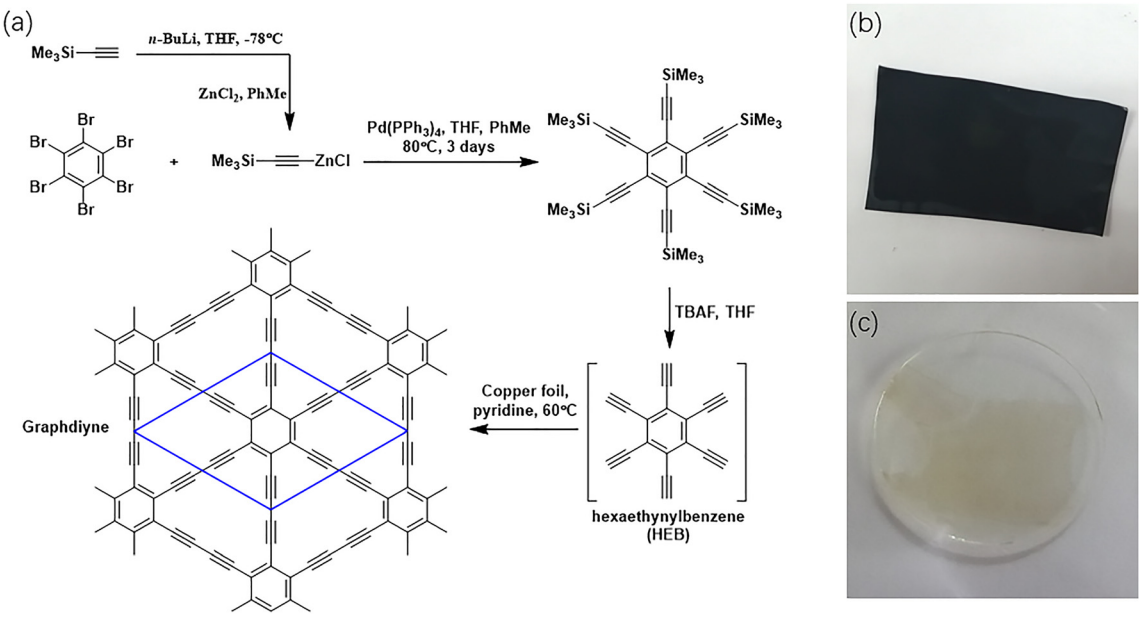

Figure 7: (a) The synthetic route for graphdiyne. (b) The graphdiyne film on copper foil. (c) The graphdiyne film after the liquid-phase exfoliation.

Finally the liquid-phase exfoliation was used in the $FeCl_3$ solution to afford the light yellow membrane, graphdiyne nanosheet [57] as shown in Figure 7c.

The photoresponse performance was tested with a photoelectrochemical test system in condition of 0.5 M KCl electrolyte. This system includes three electrodes where the graphdiyne nanosheets adhered to ITO was regarded as the working electrode (photoanode), the platinum wire was regarded as the counter electrode (cathode) and the saturated calomel electrode was regarded as the reference electrode. The substrate of the working electrode in this paper was employed by an indium-tin oxide (ITO) conductor glass with the size of $20 \times 10 \times 1\ mm^3$. After ultrasonically washed by acetone, ethanol and deionized water in turn, the ITO glass was covered by the mixed slurry of 1 mg exfoliated graphdiyne nanosheets and 1 mL NMP solution with 0.1 mg PVDF. The working electrode was dried for 12 h, yielding a catalyst loading of about 0.5 mg/cm^2 on the ITO glass. The PEC test was carried out with the present samples at a scan rate of 10 mV/s in condition of the KCl solution concentration of 0.1 M. The photocurrent can be generated under the regulation of bias potential with the electrochemistry workstation CHI660E (CH Instruments, Inc., Shanghai). A 350W Xenon arc lamp was introduced to simulate sunlight illumination with the light intensity of 100 $mW{\cdot}cm^{-2}$. The EIS test was carried out in condition of open-circuit potential with perturbation amplitude of 5 mV and the frequency from 100 kHz to 0.01 Hz. All the tests were implemented on equal terms.

Acknowledgements: P. Yin and W.L. Bao contributed equally to this work. S.R. Wei contributed the simulation analysis part. L.F. Gao contributed the modification of characters part. Authors also acknowledge the support from Instrumental Analysis Center of Shenzhen University (Xili Campus).

Author contributions: All the authors have accepted responsibility for the entire content of this submitted manuscript and approved submission.

Research funding: The research was partially supported by the National Natural Science Fund (Grant Nos. 62005177, 61875138, 61435010, and 61961136001), and Science and Technology Innovation Commission of Shenzhen (KQTD20 15032416270385, JCYJ20170811093453105, JCYJ20180307164 612205, and GJHZ20180928160209731).

Conflict of interest statement: The authors declare no conflicts of interest regarding this article.

References

[1] X. Wang, Z. Cheng, K. Xu, H. K. Tsang, and J. -B. Xu, "High-responsivity graphene/silicon-heterostructure waveguide photodetectors," *Nat. Photonics*, vol. 7, no. 11, p. 888, 2013.

[2] J. Park, Y. H. Ahn, and C. R. Vargas, "Imaging of photocurrent generation and collection in single-layer graphene," *Nano Lett.*, vol. 9, no. 5, pp. 1742–1746, 2009.

[3] B. R. Matis, J. S. Burgess, F. A. Bulat, A. L. Friedman, B. H. Houston, and J. W. Baldwin, "Surface doping and band gap tunability in hydrogenated graphene," *ACS Nano*, vol. 6, no. 1, pp. 17–22, 2012.

[4] Y. Zhang, T. Liu, B. Meng, et al., "Broadband high photoresponse from pure monolayer graphene photodetector," *Nat. Commun.*, vol. 4, p. 1911, 2013.

[5] C. M. Park and H. J. Sohn, "Black phosphorus and its composite for lithium rechargeable batteries," *Adv. Mater.*, vol. 19, no. 18, pp. 2465–2468, 2007.
[6] N. Youngblood, C. Chen, S. J. Koester, and M. Li, "Waveguide-integrated black phosphorus photodetector with high responsivity and low dark current," *Nat. Photonics*, vol. 9, no. 4, p. 247, 2015.
[7] H. Yuan, X. Liu, F. Afshinmanesh, et al., "Polarization-sensitive broadband photodetector using a black phosphorus vertical *p–n* junction," *Nat. Nanotechnol.*, vol. 10, no. 8, p. 707, 2015.
[8] X. Ren, Z. Li, Z. Huang, et al., "Environmentally robust black phosphorus nanosheets in solution: application for self-powered photodetector," *Adv. Funct. Mater.*, vol. 27, no. 18, p. 1606834, 2017.
[9] C. Tan, X. Cao, X. Wu, et al., "Recent advances in ultrathin two-dimensional nanomaterials," *Chem. Rev.*, vol. 117, no. 9, pp. 6225–6331, 2017.
[10] S. Cui, H. Pu, S. A. Wells, et al., "Ultrahigh sensitivity and layer-dependent sensing performance of phosphorene-based gas sensors," *Nat. Commun.*, vol. 6, p. 8632, 2015.
[11] C. Carmen, M. Martinez, Z. Sofer, and M. Pumera, "Layered black phosphorus as a selective vapor sensor," *Angew. Chem. Int. Ed.*, vol. 54, no. 48, pp. 14317–14320, 2015.
[12] J. Sun, G. Zheng, H. W. Lee, et al., "Formation of stable phosphorus–carbon bond for enhanced performance in black phosphorus nanoparticle–graphite composite battery anodes," *Nano Lett.*, vol. 14, no. 8, pp. 4573–4580, 2014.
[13] W. Li, Y. Yang, G. Zhang, and Y. W. Zhang, "Ultrafast and directional diffusion of lithium in phosphorene for high-performance lithium-ion battery," *Nano Lett.*, vol. 15, no. 3, pp. 1691–1697, 2015.
[14] J. Dai and X. C. Zeng, "Bilayer phosphorene: effect of stacking order on bandgap and its potential applications in thin-film solar cells," *J. Phys. Chem. Lett.*, vol. 5, no. 7, pp. 1289–1293, 2014.
[15] W. Hu, L. Lin, C. Yang, J. Dai, and J. Yang, "Edge-modified phosphorene nanoflake heterojunctions as highly efficient solar cells," *Nano Lett.*, vol. 16, no. 3, pp. 1675–1682, 2016.
[16] W. Chen, J. Ouyang, H. Liu, et al., "Black phosphorus nanosheet-based drug delivery system for synergistic photodynamic/photothermal/chemotherapy of cancer," *Adv. Mater.*, vol. 29, no. 5, p. 1603864, 2017.
[17] M. Qiu, D. Wang, W. Liang, et al., "Novel concept of the smart NIR-light–controlled drug release of black phosphorus nanostructure for cancer therapy," *Proc. Natl. Acad. Sci. USA*, vol. 115, no. 3, pp. 501–506, 2018.
[18] J. Shao, C. Ruan, H. Xie, Z. Li, and X. F. Yu, "Black-phosphorus-incorporated hydrogel as a sprayable and biodegradable photothermal platform for postsurgical treatment of cancer," *Adv. Sci.*, vol. 5, no. 5, p. 1700848, 2018.
[19] S. Das, W. Zhang, M. Demarteau, A. Hoffmann, M. Dubey, and A. Roelofs, "Tunable transport gap in phosphorene," *Nano Lett.*, vol. 14, no. 10, pp. 5733–5739, 2014.
[20] F. Xia, H. Wang, and Y. Jia, "Rediscovering black phosphorus as an anisotropic layered material for optoelectronics and electronics," *Nat. Commun.*, vol. 5, no. 4458, pp. 1–6, 2014.
[21] H. Liu, A. T. Neal, Z. Zhu, et al., "Phosphorene: an unexplored 2D semiconductor with a high hole mobility," *ACS Nano*, vol. 8, no. 4, pp. 4033–4041, 2014.
[22] L. Li, Y. Yu, G. J. Ye, et al., "Black phosphorus field-effect transistors," *Nat. Nanotechnol.*, vol. 9, no. 5, p. 372, 2014.
[23] A. Favron, E. Gaufrès, F. Fossard, et al., "Photooxidation and quantum confinement effects in exfoliated black phosphorus," *Nat. Mater.*, vol. 14, no. 8, p. 826, 2015.
[24] Q. Wang, K. Cai, J. Li, et al., "Rational design of ultralarge $Pb_{1-x}Sn_xTe$ nanoplates for exploring crystalline symmetry-protected topological transport," *Adv. Mater.*, vol. 28, no. 4, pp. 617–623, 2016.
[25] Q. Zhou, Q. Chen, Y. Tong, and J. Wang, "Light-induced ambient degradation of few-layer black phosphorus: mechanism and protection," *Angew. Chem. Int. Ed.*, vol. 55, no. 38, pp. 11437–11441, 2016.
[26] J. D. Wood, S. A. Wells, D. Jariwala, et al., "Effective passivation of exfoliated black phosphorus transistors against ambient degradation," *Nano Lett.*, vol. 14, no. 12, pp. 6964–6970, 2014.
[27] R. A. Doganov, E. C. T. O'Farrell, S. P. Koenig, et al., "Transport properties of pristine few-layer black phosphorus by van der Waals passivation in an inert atmosphere," *Nat. Commun.*, vol. 6, p. 6647, 2015.
[28] Y. Zhao, H. Wang, H. Huang, et al., "Surface coordination of black phosphorus for robust air and water stability," *Angew. Chem. Int. Ed.*, vol. 55, no. 16, pp. 5003–5007, 2016.
[29] Z. Guo, S. Chen, Z. Wang, et al., "Metal-ion-modified black phosphorus with enhanced stability and transistor performance," *Adv. Mater.*, vol. 29, no. 42, p. 1703811, 2017.
[30] X. Tang, W. Liang, J. Zhao, et al., "Fluorinated phosphorene: electrochemical synthesis, atomistic fluorination, and enhanced stability," *Small*, vol. 13, no. 47, p. 1702739, 2017.
[31] C. R. Ryder, J. D. Wood, S. A. Wells, et al., "Covalent functionalization and passivation of exfoliated black phosphorus via aryl diazonium chemistry," *Nat. Chem.*, vol. 8, no. 6, p. 597, 2016.
[32] H. Huang, X. Ren, Z. Li, et al., "Two-dimensional bismuth nanosheets as prospective photo-detector with tunable optoelectronic performance," *Nanotechnology*, vol. 29, no. 23, p. 235201, 2018.
[33] W. Huang, C. Xing, Y. Wang, et al., "Facile fabrication and characterization of two-dimensional bismuth (III) sulfide nanosheets for high-performance photodetector applications under ambient conditions," *Nanoscale*, vol. 10, no. 5, pp. 2404–2412, 2018.
[34] Z. Li, H. Qiao, Z. Guo, et al., "High-performance photo-electrochemical photodetector based on liquid-exfoliated few-layered InSe nanosheets with enhanced stability," *Adv. Funct. Mater.*, vol. 28, no. 16, p. 1705237, 2018.
[35] Z. Xie, C. Xing, W. Huang, et al., "Ultrathin 2D nonlayered tellurium nanosheets: facile liquid-phase exfoliation, characterization, and photoresponse with high performance and enhanced stability," *Adv. Funct. Mater.*, vol. 28, no. 16, p. 1705833, 2018.
[36] C. Xing, W. Huang, Z. Xie, et al., "Ultrasmall bismuth quantum dots: facile liquid-phase exfoliation, characterization, and application in high-performance UV–Vis photodetector," *ACS Photonics*, vol. 5, no. 2, pp. 621–629, 2017.
[37] I. Pletikosić, F. V. Rohr, P. Pervan, et al., "Band structure of the IV–VI black phosphorus analog and thermoelectric SnSe," *Phys. Rev. Lett.*, vol. 120, no. 15, p. 156403, 2018.
[38] L. Gao, R. Wang, A. V. Kuklin, H. Zhang, and H. Ågren, "PbSe nanocrystals produced by facile liquid phase exfoliation for efficient UV–Vis photodetectors," *Adv. Funct. Mater.*, vol. 31, no. 17, p. 2010401, 2021.

[39] L. Gao, H. Chen, R. Wang, et al., "Ultra-small 2D PbS nanoplatelets: liquid-phase exfoliation and emerging applications for photo-electrochemical photodetectors," *Small*, vol. 17, no. 5, p. 2005913, 2021.
[40] D. Kufer, I. Nikitskiy, T. Lasanta, G. Navickaite, F. H. L. Koppens, and G. Konstantatos, "Hybrid 2D–0D MoS_2–PbS quantum dot photodetectors," *Adv. Mater.*, vol. 27, no. 1, pp. 176–180, 2015.
[41] R. Lv, J. A. Robinson, R. E. Schaak, et al., "Transition metal dichalcogenides and beyond: synthesis, properties, and applications of single-and few-layer nanosheets," *Acc. Chem. Res.*, vol. 48, no. 1, pp. 56–64, 2014.
[42] Y. Zhang, T. R. Chang, B. Zhou, et al., "Direct observation of the transition from indirect to direct bandgap in atomically thin epitaxial $MoSe_2$," *Nat. Nanotechnol.*, vol. 9, no. 2, p. 111, 2014.
[43] L. Gao, C. Li, W. Huang, et al., "MXene/polymer membranes: synthesis, properties, and emerging applications," *Chem. Mater.*, vol. 32, no. 5, pp. 1703–1747, 2020.
[44] T. Yang, L. Gao, W. Wang, et al., "Berlin green framework-based gas sensor for room-temperature and high-selectivity detection of ammonia," *Nano-Micro Lett.*, vol. 13, no. 1, p. 63, 2021.
[45] Q. Tian, P. Yin, T. Zhang, et al., "MXene $Ti_3C_2T_x$ saturable absorber for passively Q-switched mid-infrared laser operation of femtosecond-laser-inscribed Er:Y_2O_3 ceramic channel waveguide," *Nanophotonics*, vol. 9, no. 8, p. 2495, 2020 (in English).
[46] C. Ma, P. Yin, K. Khan, et al., "Broadband nonlinear photonics in few-layer borophene," *Small*, vol. 17, no. 7, p. 2006891, 2021.
[47] C. Tan and H. Zhang, "Wet-chemical synthesis and applications of non-layer structured two-dimensional nanomaterials," *Nat. Commun.*, vol. 6, p. 7873, 2015.
[48] Q. Wang, K. Xu, Z. Wang, et al., "Van der Waals epitaxial ultrathin two-dimensional nonlayered semiconductor for highly efficient flexible optoelectronic devices," *Nano Lett.*, vol. 15, no. 2, pp. 1183–1189, 2015.
[49] F. Wang, Z. Wang, T. A. Shifa, et al., "Two-dimensional non-layered materials: synthesis, properties and applications," *Adv. Funct. Mater.*, vol. 27, no. 19, p. 1603254, 2017.
[50] J. Song Chen, D. Luan, C. M. Li, F. Y. C. Boey, S. Qiao, and X. Wen Lou, "TiO_2 and SnO_2@TiO_2 hollow spheres assembled from anatase TiO_2 nanosheets with enhanced lithium storage properties," *Chem. Commun.*, vol. 46, no. 43, pp. 8252–8254, 2010.
[51] Y. Sun, Z. Sun, S. Gao, et al., "Fabrication of flexible and freestanding zinc chalcogenide single layers," *Nat. Commun.*, vol. 3, p. 1057, 2012.
[52] Y. Xu, W. Zhao, R. Xu, Y. Shia, and B. Zhang, "Synthesis of ultrathin CdS nanosheets as efficient visible-light-driven water splitting photocatalysts for hydrogen evolution," *Chem. Commun.*, vol. 49, no. 84, pp. 9803–9805, 2013.
[53] J. Zhu, L. Bai, Y. Sun, et al., "Topochemical transformation route to atomically thick Co_3O_4 nanosheets realizing enhanced lithium storage performance," *Nanoscale*, vol. 5, no. 12, pp. 5241–5246, 2013.
[54] F. Wang, J. H. Seo, G. Luo, et al., "Nanometre-thick single-crystalline nanosheets grown at the water–air interface," *Nat. Commun.*, vol. 7, p. 10444, 2016.
[55] Q. Wang, Y. Wen, F. Yao, et al., "BN-enabled epitaxy of $Pb_{1-x}Sn_xSe$ nanoplates on SiO_2/Si for high-performance mid-infrared detection," *Small*, vol. 11, no. 40, pp. 5388–5394, 2015.
[56] A. Hirsch, "The era of carbon allotropes," *Nat. Mater.*, vol. 9, no. 11, pp. 868–871, 2010.
[57] G. Li, Y. Li, H. Liu, Y. Guo, Y. Lia, and D. Zhu, "Architecture of graphdiyne nanoscale films," *Chem. Commun.*, vol. 46, no. 19, pp. 3256–3258, 2010.
[58] G. Luo, X. Qian, H. Liu et al., "Quasiparticle energies and excitonic effects of the two-dimensional carbon allotrope graphdiyne: theory and experiment," *Phys. Rev. B*, vol. 84, no. 7, p. 075439, 2011.
[59] C. Huang, Y. Li, N. Wang, et al., "Progress in research into 2D graphdiyne-based materials," *Chem. Rev.*, vol. 118, no. 16, pp. 7744–7803, 2018.
[60] X. Gao, H. Liu, D. Wang, and J. Zhang, "Graphdiyne: synthesis, properties, and applications," *Chem. Soc. Rev.*, vol. 48, no. 3, pp. 908–936, 2019.
[61] Y. Du, W. Zhou, J. Gao, X. Pan, and Y. Li, "Fundament and application of graphdiyne in electrochemical energy," *Acc. Chem. Res.*, vol. 53, no. 2, pp. 459–469, 2020.
[62] Z. Zuo, and Y. Li, "Emerging electrochemical energy applications of graphdiyne," *Joule*, vol. 3, no. 4, pp. 899–903, 2019.
[63] L. Li, Z. Zuo, F. Wang, et al., "In situ coating graphdiyne for high-energy-density and stable organic cathodes," *Adv. Mater.*, vol. 32, no. 14, p. 2000140, 2020.
[64] Y. Fang, Y. Xue, Y. Li, et al., "Graphdiyne interface engineering: highly active and selective ammonia synthesis," *Angew. Chem. Int. Ed.*, vol. 59, no. 31, pp. 13021–13027, 2020.
[65] Y. Fang, Y. Xue, L. Hui, H. Yu, and Y. Li, "Graphdiyne@Janus magnetite for photocatalytic nitrogen fixation," *Angew. Chem. Int. Ed.*, vol. 60, no. 6, pp. 3170–3174, 2021.
[66] Y. Xue, B. Huang, Y. Yi, et al., "Anchoring zero valence single atoms of nickel and iron on graphdiyne for hydrogen evolution," *Nat. Commun.*, vol. 9, no. 1, p. 1460, 2018.
[67] L. Hui, Y. Xue, H. Yu, et al., "Highly efficient and selective generation of ammonia and hydrogen on a graphdiyne-based catalyst," *J. Am. Chem. Soc.*, vol. 141, no. 27, pp. 10677–10683, 2019.
[68] L. Wu, Y. Dong, J. Zhao, et al., "Kerr nonlinearity in 2D graphdiyne for passive photonic diodes," *Adv. Mater.*, vol. 31, no. 14, p. 1807981, 2019.
[69] Y. I. Jhon, Y. T. Byun, J. H. Lee, and Y. M. Jhon, "Robust mechanical tunability of 2D transition metal carbides via surface termination engineering: molecular dynamics simulation," *Appl. Surf. Sci.*, vol. 532, p. 147380, 2020.
[70] Y. Li, Q. Liu, W. Li, H. Meng, Y. Lu, and C. Li, "Synthesis and supercapacitor application of alkynyl carbon materials derived from CaC_2 and polyhalogenated hydrocarbons by interfacial mechanochemical reactions," *ACS Appl. Mater. Interfaces*, vol. 9, no. 4, pp. 3895–3901, 2017.
[71] Y. Li, Q. Liu, W. Li, H. Meng, Y. Lu, and C. Li, "Efficient destruction of hexachlorobenzene by calcium carbide through mechanochemical reaction in a planetary ball mill," *Chemosphere*, vol. 166, pp. 275–280, 2017.
[72] R. Matsuoka, R. Sakamoto, K. Hoshiko, et al., "Crystalline graphdiyne nanosheets produced at a gas/liquid or liquid/liquid interface," *J. Am. Chem. Soc.*, vol. 139, no. 8, pp. 3145–3152, 2017.
[73] Y. K. Ke and H. R. Dong, *Molecular Spectroanalysis Handbook of Analytical Chemistry*, Beijing, Chemical Industry Press, 2016, pp. 537–538.

[74] M. A. Aguado, M. A. Anderson, and C. G. Hill, "Influence of light intensity and membrane properties on the photocatalytic degradation of formic acid over TiO_2 ceramic membranes," *J. Mol. Catal.*, vol. 89, pp. 165–178, 1994.
[75] H. Qiao, J. Yuan, Z. Xu, et al., "Broadband photodetectors based on graphene–Bi_2Te_3 heterostructure," *ACS Nano*, vol. 9, no. 2, pp. 1886–1894, 2015.
[76] X. Ren, Q. Xiang, Y. Shen, X. Si, and J. Zhong, "2D co-catalytic MoS_2 nanosheets embedded with 1D TiO_2 nanoparticles for enhancing photocatalytic activity," *J. Phys. D Appl. Phys.*, vol. 49, no. 31, p. 315304, 2016.
[77] Q. Hong, Y. Cao, J. Xu, H. Lu, J. He, and J. L. Sun, "Self-powered ultrafast broadband photodetector based on *p–n* heterojunctions of CuO/Si nanowire array," *ACS Appl. Mater. Interfaces*, vol. 6, no. 23, pp. 20887–20894, 2014.
[78] R. J. Candal, W. A. Zeltner, and M. A. Anderson, "Effects of pH and applied potential on photocurrent and oxidation rate of saline solutions of formic acid in a photoelectrocatalytic reactor," *Environ. Sci. Technol.*, vol. 34, no. 16, pp. 3443–3451, 2000.
[79] M. Huang, M. Wang, C. Chen, et al., "Broadband black-phosphorus photodetectors with high responsivity," *Adv. Mater.*, vol. 28, no. 18, pp. 3481–3485, 2016.
[80] J. Miao, S. Zhang, L. Cai, and C. Wang, "Black phosphorus Schottky diodes: channel length scaling and application as photodetectors," *Adv. Electron. Mater.*, vol. 2, no. 4, p. 1500346, 2016.
[81] M. Buscema, D. J. Groenendijk, S. I. Blanter, G. A. Steele, H. S. van der Zant, and A. C. Gomez, "Fast and broadband photoresponse of few-layer black phosphorus field-effect transistors," *Nano Lett.*, vol. 14, no. 6, pp. 3347–3352, 2014.
[82] W. Zhang, M.-H. Chiu, C.-H. Chen, W. Chen, L.-J. Li, and A. T. S. Wee, "Role of metal contacts in high-performance phototransistors based on WSe_2 monolayers," *ACS Nano*, vol. 8, no. 8, pp. 8653–8661, 2014.
[83] O. L. Sanchez, D. Lembke, M. Kayci, A. Radenovic, and A. Kis, "Ultrasensitive photodetectors based on monolayer MoS_2," *Nat. Nanotechnol.*, vol. 8, no. 7, pp. 497–501, 2013.
[84] Z. Yin, H. Li, H. Li, et al., "Single-layer MoS_2 phototransistors," *ACS Nano*, vol. 6, no. 1, pp. 74–80, 2012.
[85] Y. Xue, Y. Zhang, Y. Liu, et al., "Scalable production of a few-layer MoS_2/WS_2 vertical heterojunction array and its application for photodetectors," *ACS Nano*, vol. 10, no. 1, pp. 573–580, 2016.
[86] L. Gao, C. Ma, S. Wei, A. V. Kuklin, H. Zhang, and H. Ågren, "Applications of few-layer Nb_2C MXene: narrow-band photodetectors and femtosecond mode-locked fiber lasers," *ACS Nano*, vol. 15, no. 1, pp. 954–965, 2021.
[87] B. Chitara, S. B. Krupanidhi, and C. N. R. Rao, "Solution processed reduced graphene oxide ultraviolet detector," *Appl. Phys. Lett.*, vol. 99, no. 11, 2011, https://doi.org/10.1063/1.3640222.
[88] W. Liu, X. Yan, J. Lang, and Q. Xue, "Effects of concentration and temperature of EMIMBF4/acetonitrile electrolyte on the supercapacitive behavior of graphene nanosheets," *J. Mater. Chem.*, vol. 22, no. 18, pp. 8853–8861, 2012.
[89] A. O. King, E. Negishi, F. J. Villani, and A. Silveira, "A general synthesis of terminal and internal arylalkynes by the palladium-catalyzed reaction of alkynylzinc reagents with aryl halides," *J. Org. Chem.*, vol. 43, no. 2, pp. 358–360, 1978.